Lithos 336–337 (2019) 54–66

Contents lists available at ScienceDirect

Lithos

journal homepage: www.elsevier.com/locate/lithos

Contrasting whole-rock and mineral compositions of ore-bearing (Tongchang) and ore-barren (Shilicun) granitic plutons in SW China: Implications for petrogenesis and ore genesis

Lei-Luo Xu [a,b,*], Xian-Wu Bi [a,*], Rui-Zhong Hu [a], Yong-Yong Tang [a], Xin-Song Wang [a], Ming-Liang Huang [a,c], Ying-Jing Wang [a,c], Rui Ma [a,c], Gong Liu [a,c]

[a] State Key Laboratory of Ore Deposit Geochemistry, Institute of Geochemistry, Chinese Academy of Sciences, Guiyang 550081, China
[b] EGRU (Economic Geology Research Center), James Cook University, Townsville 4811, Australia
[c] University of Chinese Academy of Sciences, Beijing 100049, China

ARTICLE INFO

Article history:
Received 29 August 2018
Accepted 27 March 2019
Available online 1 April 2019

Keywords:
Porphyry Cu ± Mo ± au ores
Granitic pluton
Petrogenesis
Ore genesis
SW China

ABSTRACT

A common perception is that oxidized magma is critical for the formation of a porphyry Cu ± Mo ± Au ore deposit. We have used an ore-bearing pluton (Tongchang) and an ore-barren pluton (Shilicun) in the western rim of the South China block to test this idea and to determine other important controls on ore genesis. Zircon U—Pb ages indicate that the Tongchang and Shilicun plutons were emplaced at 36.3 ± 0.2 Ma and 35.2 ± 0.4 Ma, respectively, broadly coinciding with strike-slip faulting in the region and continental collision that occurred ~300 km to the west. These two plutons are all characterized by significant light REE enrichments and pronounced negative Nb—Ta anomalies, similar to the bulk crust. Apatite separates from these two plutons all have elevated initial $^{87}Sr/^{86}Sr$ (Tongchang, 0.70690 to 0.70796; Shilicun, 0.70703 to 0.70726) and negative $\varepsilon_{Nd}(t)$ (Tongchang, −6.2 to −7.3; Shilicun, −4.5 to −5.8). The mean $\varepsilon_{Hf}(t)$ and $\delta^{18}O$ of zircon from these plutons are −1.4 and 6.8‰ for Tongchang, and −0.3 and 6.5‰ for Shilicun. The Sr-Nd-Hf isotope compositions are all within the ranges of the Neoproterozoic mafic arc lower crust in the region. Whole-rock U-Nb-Ta systematics indicate that the Tongchang and Shilicun plutons originated from an amphibole-bearing source and a garnet-bearing source, respectively, implying a shallower and more H_2O-rich mafic source for the former than the latter. Quartz trace element data indicate that the Tongchang pluton was emplaced at a shallower depth than the Shilicun pluton. Zircon Ce^{4+}/Ce^{3+} and whole-rock V/Sc ratios, and apatite SO_3 and MnO contents indicate that the parental magmas of both plutons are as oxidized as those of some porphyry Cu deposits in northern Chile, but the parental magma of the Tongchang pluton is less oxidized than that of the Shilicun pluton. Apatite Cl-F-OH systematics and higher abundant hydrous silicate minerals such as amphibole and biotite in the Tongchang pluton than the Shilicun pluton indicate that the parental magma of the Tongchang pluton has higher Cl and H_2O content than that of the Shilicun pluton. Our results show that oxidized magma is important but this alone cannot make a porphyry Cu ± Mo ± Au ore deposit. High contents of H_2O-Cl in magma and shallow depth of emplacement are also important.

1. Introduction

It is well known that most porphyry Cu ± Mo ± Au ore deposits in the world are associated with oxidized intermediate-felsic magmas (Ballard et al., 2002; Mungall, 2002; Richards, 2011b, 2015; Richards and Celâl Şengör, 2017; Sillitoe, 2010). Perhaps this is because under oxidized condition the ore metals such as Cu, Mo and Au can be more easily transported by magma to upper crustal levels and become highly concentrated in the ore-forming magmatic fluids (Ballard et al., 2002; Richards, 2011b, 2015; Richards and Celâl Şengör, 2017). Many researchers have studied the oxidation states of porphyry Cu ± Mo ± Au ore deposits and found that in a given region the parental magmas of ore-bearing plutons tend to be more oxidized than those of generally coeval ore-barren plutons (e.g., Ballard et al., 2002; Bi et al., 2009; Liang et al., 2006; Lu et al., 2016; Shen et al., 2015; Sun et al., 2015, 2017; Wang et al., 2014a, 2014b, 2018; Xu et al., 2016a; Zhang et al., 2017).

Eocene intermediate-felsic plutons are widely distributed in the western rim of the South China block (Fig. 1a, b). Some of these plutons host important porphyry-skarn Cu ± Mo ± Au ore deposits such as the

* Corresponding authors at: State Key Laboratory of Ore Deposit Geochemistry, Institute of Geochemistry, Chinese Academy of Sciences, Guiyang 550081, China.
E-mail addresses: xuleiluo@vip.gyig.ac.cn (L.-L. Xu), bixianwu@vip.gyig.ac.cn (X.-W. Bi).

https://doi.org/10.1016/j.lithos.2019.03.031
0024-4937/

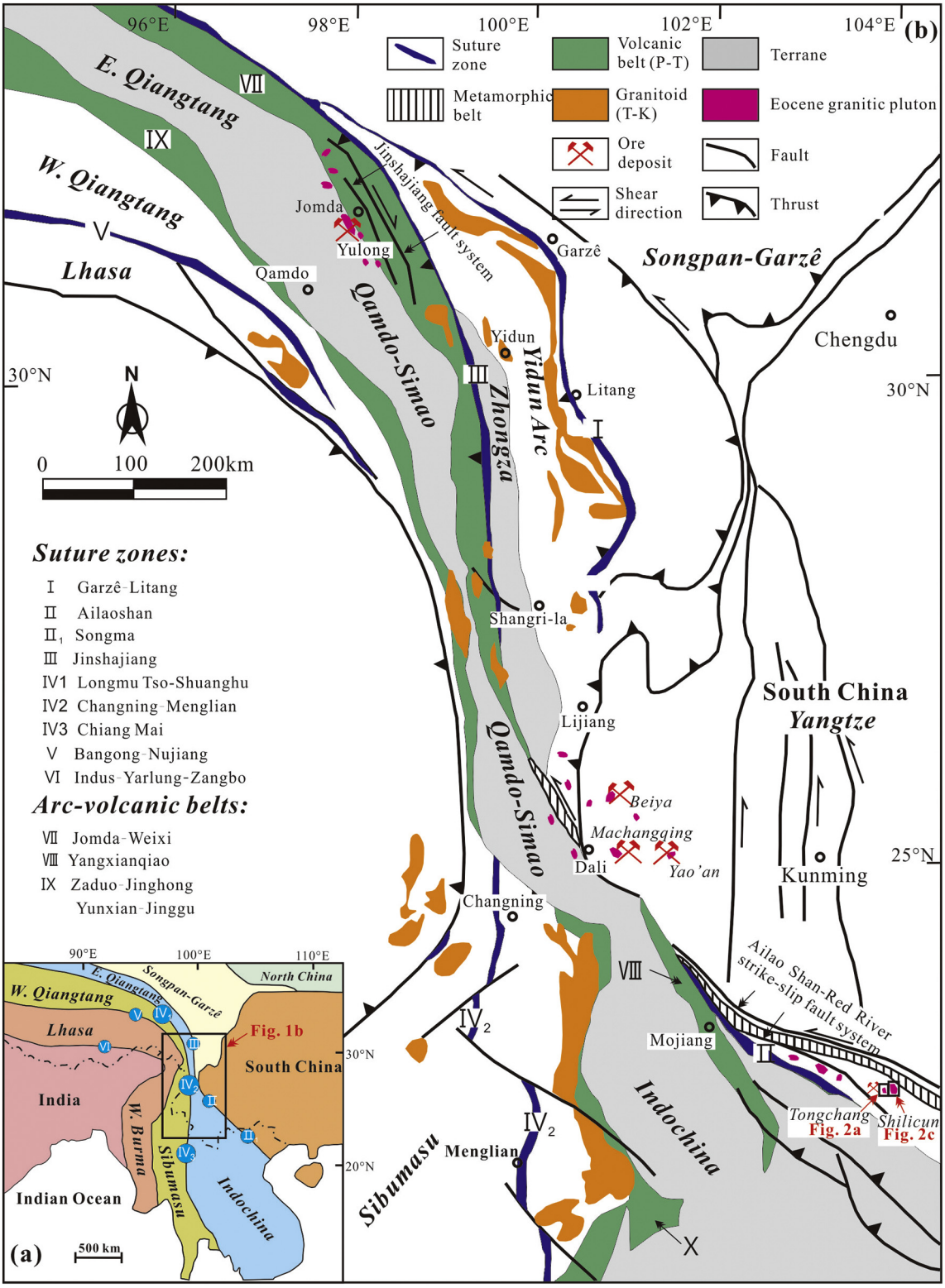

Fig. 1. (a) Distribution of principal continental blocks and sutures of southeast Asia (modified from Zhu et al., 2015); (b) tectonic framework of the Eastern Tibetan plateau and surrounding areas showing the major terranes, suture zones, arc volcanic belts, Eocene major granitic plutons and related Cu-Mo-Au deposits, and locations of the Tongchang and Shilicun granitic plutons (modified from Zhu et al., 2015).

Tongchang, Machangqing, Yao'an and Beiya deposits (Lu et al., 2013a; Xu et al., 2012, 2016a). Our recent investigation shows that the parental magmas of an ore-bearing granitic pluton (Tongchang) and a generally coeval ore-barren granitic pluton (Shilicun) in the Ailaoshan area (Figs. 1b, 2) are as oxidized as those of some porphyry Cu ore deposits in northern Chile (data from Ballard et al., 2002), but the parental magma of the Shilicun ore-barren pluton is even more oxidized than that of the Tongchang ore-bearing pluton. This implies that in addition to highly oxidized conditions, there are other important generic controls on the type of mineralization, at least in this area. Thus, we have carried out a comparative geochemical study between these two plutons to evaluate other important controls on ore genesis. New data

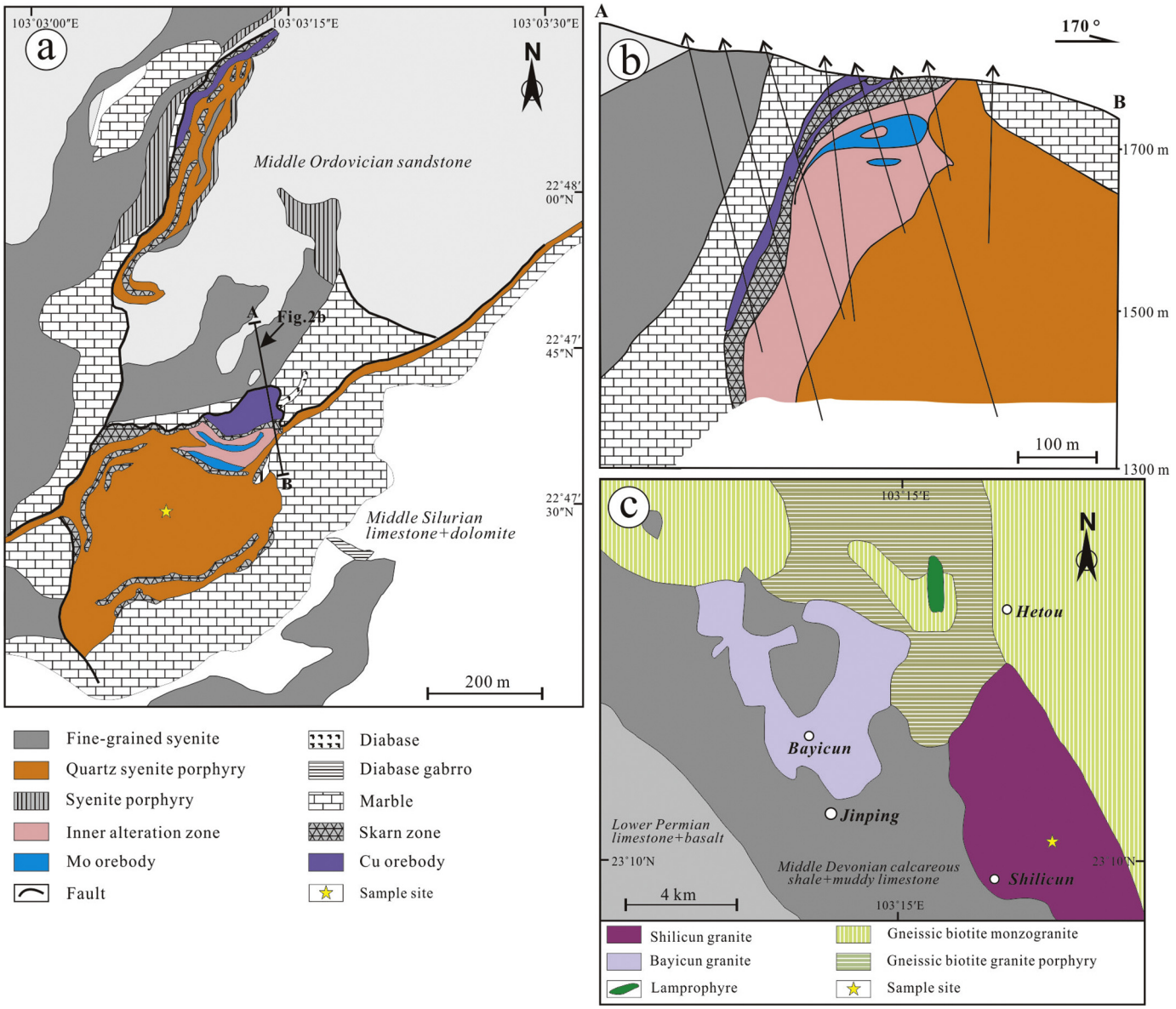

Fig. 2. (a) Simplified geological map of the Tongchang Cu-Mo(Au) deposit, and (b) representative cross section through the Tongchang deposit showing the spatial relationship among wall-rocks, pluton, skarn zone, inner alteration zone and orebodies (modified from Xu et al., 2014); (c) simplified geological map of the Shilicun granitic pluton (modified from Xie and Zhang, 1988).

from this study include whole-rock major and trace element compositions, the anorthite (An) contents of plagioclase, trace element abundances in quartz and zircon, a U–Pb age and the Hf–O isotopes of zircon, and the chemical composition and Sr–Nd isotopes of apatite. The results and new findings are reported in the paper.

2. Regional geological setting and pluton geology

2.1. Regional geological setting

The Tethyan tectonic domain in China, which stretches from Tibet to western Yunnan, encompasses a series of arc terranes and micro-continental blocks such as Songpan-Ganze, Qiangtang, Lhasa, Tengchong, Baoshan and Simao that were accreted to the Eurasian main continent prior to Late Cretaceous (Fig. 1; Hu et al., 2004; Hou et al., 2007). In the Sanjiang region, the Tethyan domain is bounded by the Indian continent to the west and by the South China block to the east. The eastern suture formed in Early Triassic as the result of Paleo-Tethyan Ocean closure by westward subduction whereas the western suture formed much latter in the Cenozoic as the results of Neo-Tethyan Ocean closure by eastward subduction (Deng et al., 2014a). The initial collision between the Indian continent and the Lhasa block, which is commonly referred to as the Indo-Asian collision, took place at ~65 Ma (Hou et al., 2006, 2007; Hu et al., 2004). This collision event was protracted and produced a series of major overthrusts and strike-slip faults in the Sanjiang region such as Jinshajiang shear zone and the adjacent western rim of South China block such as the Red River-Ailaoshan shear zone (Deng et al., 2014b). Between ~40 and ~30 Ma numerous ultra-potassic mafic to felsic dykes and many granitic plutons were emplaced in the greater Sanjiang region including the western rim of the South China block (Lu et al., 2012; Zhang and Xie, 1997). Some of the granitic plutons in the Jinshajiang and Red River-Ailaoshan regions host porphyry Cu—Mo (Au) ore deposits (Hou et al., 2006; Xu et al., 2012).

2.2. Pluton geology

The Tongchang ore-bearing granitic pluton is located in the Ailaoshan area in the southwestern rim of the South China block. This pluton hosts a major porphyry Cu—Mo (Au) ore deposit (Fig. 1b). The Tongchang granitic pluton is composed of quartz syenite porphyries. It is exposed in a small area of ~0.2 km^2. The wall rocks of this pluton are Middle Silurian limestones and sandstones, and Middle Ordovician sandstones (Fig. 2a). The quartz syenite porphyries have a porphyritic texture with phenocrysts of K-feldspar (~50–60 vol%), plagioclase (~20–30 vol%), quartz (~10–15 vol%), amphibole (~5–10 vol%) and biotite (~1–5 vol%) in a cryptocrystalline groundmass (Fig. 3a). Zircon, apatite and titanite are the principal accessory minerals.

The Tongchang porphyry Cu—Mo (Au) ore deposit contains ~8621 metric tons (t) Cu and 17,060 t Mo, with averages grades of 1.24 wt% Cu, 0.218 wt% Mo and 0.13 g/t Au. From the inner part of the quartz syenite porphyry pluton through the contact to the wall-rock, three mineralization-related alteration zones are present, namely the inner alteration zone, the skarn zone and the outer alteration zone (Xu et al., 2014). The inner alteration zone has a mineral assemblage that is very similar to those of typical porphyry Cu—Mo ore systems (Sillitoe, 2010): pervasive K-silicate and quartz-sericite alteration with disseminated molybdenite ± chalcopyrite and veinlets of molybdenite ± chalcopyrite (Fig. 2a, b). The skarn zone mainly occurs in the contact between the pluton and Middle Silurian limestone (Fig. 2a, b), and is composed of garnet, scapolite, tremolite, epidote, diopside and forsterite, with abundant Cu-sulfides and magnetite. The outer alteration zone in the wall-rocks is mainly composed of marble (Fig. 2a, b), with minor serpentine, quartz, chlorite, wollastonite and clinohumite. Weak Pb—Zn and Cu—Mo sulfide mineralization is present close to the contact with the skarn zone (Xu et al., 2014).

The Shilicun ore-barren granitic pluton also occurs in the Ailaoshan area belonging to the western rim of the South China block. The distance between this ore-barren granitic pluton and the Tongchang ore-bearing granitic pluton is ~20 km (Fig. 1b). The Shilicun granitic pluton is diopside-bearing (Fig. 2c). The granitic rocks (Fig. 3b) are composed of K-feldspar (~40–50 vol%), plagioclase (~25–30 vol%), quartz (~15–20 vol%), diopside (~5 vol%) and minor amphibole, with zircon, apatite, titanite and magnetite as the principal accessory minerals (Xie and Zhang, 1988). The Shilicun granitic pluton is exposed sporadically in an area of ~25 km^2. The wall-rocks of this pluton include Triassic gneissic biotite monzogranites and gneissic biotite granite porphyries and Middle Devonian calcareous shales and muddy limestones (Fig. 2c; Xie and Zhang, 1988). No significant hydrothermal alteration and mineralization are present in the Shilicun granitic pluton and its contact with the wall-rocks (Xia et al., 2005; Xie and Zhang, 1988).

3. Analytical methods

The least altered rock samples were selected for whole-rock chemical analysis and separation of zircon and apatite. Zircon and apatite separates were separated from a large (~2 kg) rock sample using standard density and magnetic separation techniques. The mineral grains were hand-picked and mounted in epoxy resin discs, and then polished. Cathodoluminescence (CL) images of the selected grains, obtained using a Field Emission Scanning Electron Microscope (JSM-7800F, Japan Electronic Co., Ltd.) at the State Key Laboratory of Ore Deposit Geochemistry (SKLODG), Institute of Geochemistry, Chinese Academy of Sciences, Guiyang, China, were used for target selection.

3.1. Whole-rock chemical analysis

Whole-rock major element compositions were determined using a PANalytical Axios–advance (Axios PW4400) X-ray fluorescence spectrometer (XRF) at the SKLODG. The measurements were made on fused glass disks. The analytical precision, based on the results for the Chinese National standard GSR-1 and GSR-3, is better than 5%. Loss on ignition (LOI) was obtained using 1 g powder heated up to 1100 °C for 1 h.

Whole-rock trace element concentrations were determined using a Perkin-Elmer ELAN-DRC-e inductively coupled plasma mass spectrometer (ICP-MS) at the SKLODG. The powdered samples (50 mg) were dissolved in high-pressure Teflon bombs using HF + HNO_3 mixture for 48 h at ~195 °C. Rhodium was used as an internal standard to monitor signal drift during counting. The international standards GBPG-1 and OU-6, and the Chinese National standard GSR-1 were used for quality control. The analytical precision, based on the results of the standards, is better than 10%.

3.2. U—Pb dating and trace element analysis of zircon

Trace element abundances and U—Pb isotopes of zircon were obtained using the LA-ICP-MS at the SKLODG. A pulsed (Geolas) 193 nm ArF Excimer (Lambda Physik, Göttingen Germany) laser with energy density of 8 J/cm^2 and diameter of laser spot of 32 μm was used for ablation at a repetition rate of 6 Hz. Detailed analytical procedures are the same as those of Liu et al. (2010). Helium was used as a carrier gas and Argon as the take-up gas that mixed with the carrier gas via a T-connector before entering the ICP. The zircon standard 91,500 was used as a calibration standard for mass discrimination and isotope fractionation, and the NIST SRM 610 glass was used as an external standard for trace element analysis. An Agilent 7700× ICP-MS was used to acquire ion-signal intensities. Each analysis incorporated a background acquisition of approximately 20–30 s (gas blank) followed by 50 s data acquisition from the sample. Off-line selection and integration of

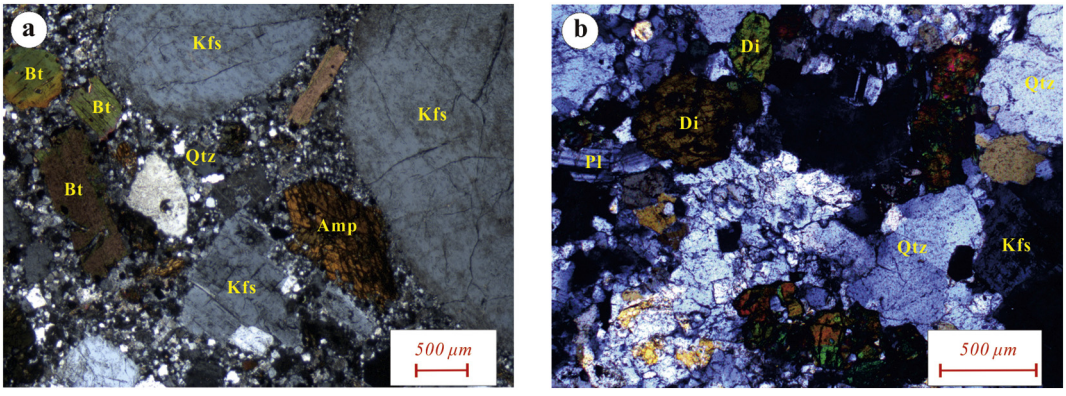

Fig. 3. Photomicrographs of the Tongchang quartz syenite porphyry (a) and Shilicun diopside granite (b). Abbreviations: Amp = amphibole, Bt = biotite, Di = diopside, Kfs = K-feldspar, Plag = plagioclase, Qtz = quartz.

background and analytical signals, and time-drift correction and quantitative calibration for zircon trace elements were performed using the ICPMSDataCal software of Liu et al. (2010).

3.3. Trace element analysis of quartz

Trace element analysis of quartz was conducted on polished thin sections of rock samples using the LA-ICP-MS at the SKLODG. A pulsed (Geolas) 193 nm ArF Excimer (Lambda Physik, Göttingen Germany) laser with energy density of 8 J/cm^2 and diameter of laser spot of 44 μm was used for ablation at a repetition rate of 10 Hz. An Agilent 7900 ICP-MS was used to acquire ion-signal intensities. Detailed analytical procedures and reduction of data are the same as those of Lan et al. (2018). A reference natural quartz crystal was analyzed to monitor the accuracy. The results for the reference (Supp. Table 3) are in good agreement with the recommended values given by Audétat et al. (2015).

3.4. Apatite-plagioclase chemical analysis and apatite Sr—Nd isotopic analysis

The chemical compositions of plagioclase and apatite were measured by wavelength dispersive X-ray analysis using an electron microprobe (EPMA-1600, Shimadu) at the SKLODG. The analytical conditions were acceleration voltage of 25 kV, beam current of 10 nA, and a beam diameter of 10 μm.

Apatite in-situ Sm—Nd isotopic analysis was carried out using a ThermoScientific Neptune MC-ICP-MS connected to a Geolas 193 nm ArF excimer laser with ablation spot diameter of 60 μm in the Advanced Analytical Centre at James Cook University (JCU), Townsville, Australia. Detailed operation conditions and analytical procedures are the same as those given in Hammerli et al. (2014). The $^{147}Sm/^{144}Nd$ ratios were calibrated against a synthetic LREE-rich silicate glass with a recommended $^{147}Sm/^{144}Nd$ of 0.2451 (Fisher et al., 2011). The $^{143}Nd/^{144}Nd$ ratios of apatite samples were normalized using the bracketing analytical results of a Nd-doped glass standard (JNdi-1), which has a recommended $^{143}Nd/^{144}Nd$ of 0.512098 ± 13 determined by TIMS (Fisher et al., 2011). The Ap1 apatite reference from Yang et al., 2014 and the Durango apatite reference were used for quality control. Our $^{143}Nd/^{144}Nd$ ratios for the Ap1 apatite are 0.511326 ± 45 (2SD, n = 4), which are in good agreement with the values (0.511349 ± 38, 2SD, n = 396) given by Yang et al., 2014. Our $^{143}Nd/^{144}Nd$ ratios for the Durango apatite are 0.512474 ± 43 (2SD, n = 7), which are in good agreement with the values 0.512489 ± 12 (2SD, n = 9) given by Fisher et al. (2011). Our $^{143}Nd/^{144}Nd$ ratios for the JNdi-1 standard are 0.512097 ± 7 (2SD, n = 8), indistinguishable from the recommended value of Fisher et al. (2011).

Apatite in-situ Rb—Sr isotopic analysis were conducted using a ThermoScientific Neptune MC-ICP-MS connected to a Geolas 193 nm ArF excimer laser with ablation spot diameter of 60 μm at the Institute of Geology and Geophysics, Chinese Academy of Sciences, Beijing, China. The samples used previously for Sm—Nd isotopic analysis were used again for the Rb—Sr isotopic analysis. Detailed operation conditions, analytical procedures and data reduction are the same as those given in Yang et al. (2014). The Ap1 apatite was used as external standard. The Slyudyanka apatite was analyzed as an unknown sample with our samples. Our $^{87}Sr/^{86}Sr$ ratios for the Slyudyanka apatite are

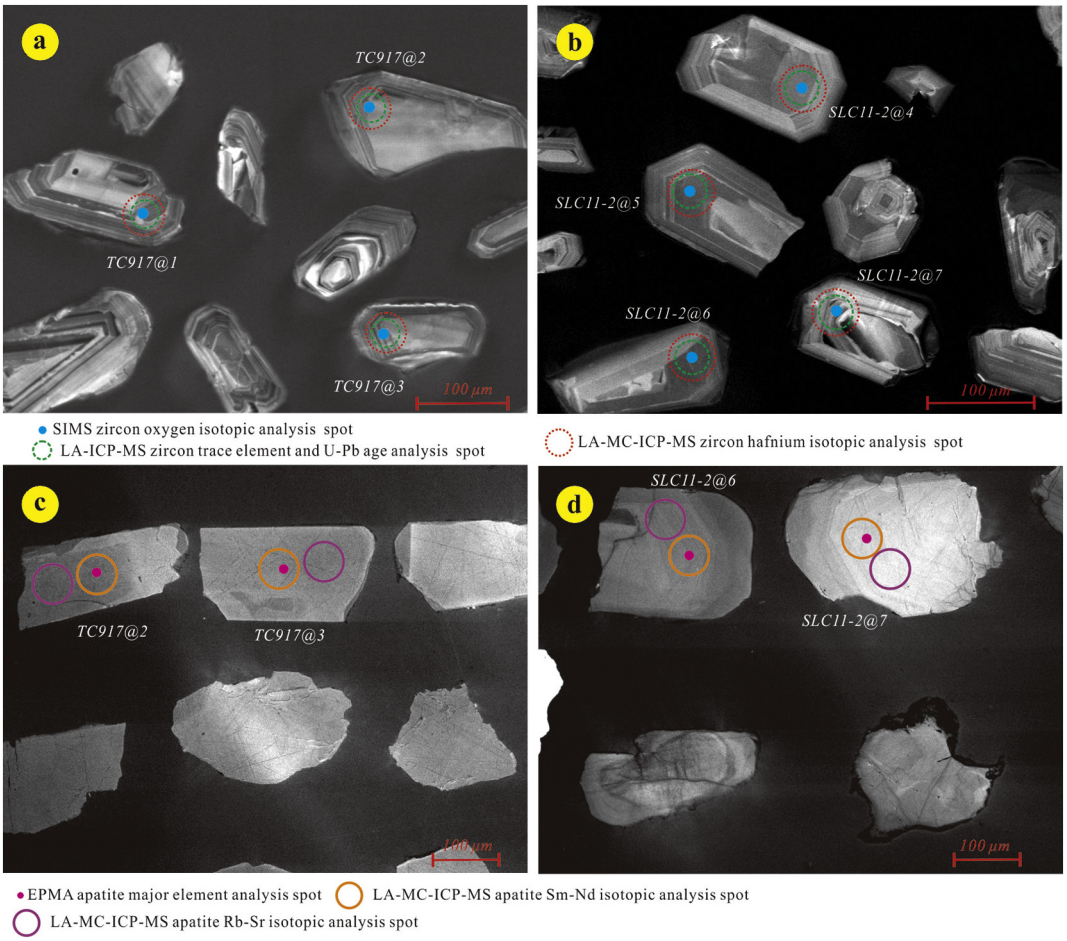

Fig. 4. Cathodoluminescence (CL) images of representative zircon grains from the Tongchang (a) and Shilicun (b) plutons, and representative apatite grains from the Tongchang (c) and Shilicun (d) plutons.

0.70771 ± 11 (2SD, n = 8), which are in good agreement with the results acquired by TIMS and solution MC-ICP-MS (0.707683 ± 25, 2SD, n = 11), and by LA-MC-ICP-MS (0.70769 ± 15, 2SD, n = 110) Yang et al. (2014). Our $^{87}Sr/^{86}Sr$ result for the Ap1 apatite are 0.71128 ± 13 (2SD, n = 8), which are in good agreement with the value determined by solution MC-ICP-MS (0.711370 ± 31, 2SD, n = 14) (Yang et al., 2014).

3.5. Zircon in-situ Hf—O isotopic analysis

Zircon oxygen isotopes were measured using a CAMECA IMS 1280 SIMS at the Institute of Geology and Geophysics, Chinese Academy of Sciences, Beijing, China. Zircon oxygen isotopic analysis was performed on the same zircon grains that were analyzed previously for trace element abundances and U—Pb ages. A Cs^+ primary ion beam was accelerated at 10 kV, with the intensity of ~2 nA and beam size of ~10 μm in diameter. Detailed operation conditions and analytical procedures are the same as those described by Li et al. (2009). The results are presented in standard delta notation: $(\delta^{18}O = ((^{18}/^{16}O)_{sample}/(^{18}O/^{16}O)_{VSMOW}) - 1$, with conversion to ‰ achieved by 1000, where $(^{18}O/^{16}O)_{V-SMOW} = 0.0020052$ (VSMOW being Vienna Standard Mean Ocean Water).

Zircon in-situ Hf isotopic analysis was carried out using a Neptune Plus MC-ICP-MS equipped with a Geolas 2005 excimer ArF laser ablation system at the state Key Laboratory of Geological Processes and Mineral Resources, China University of Geosciences (Wuhan), China. Zircon Lu—Hf isotopic measurements were made on the same zircon grains that were previously analyzed for oxygen isotopes, trace elements and U—Pb ages. The diameter of the laser spot for zircon Hf isotopic analysis was ~40 μm. Detailed operation conditions and analytical procedures are the same as those of Hu et al. (2012). Off-line selection and integration of analytical signals, and mass bias calibrations were performed using the ICPMSDataCal software of Liu et al. (2010). Our $^{176}Hf/^{177}Hf$ ratios for the zircon 91,500 standard analyzed with our samples are 0.282315 ± 19 (2SD, n = 156), which are in good agreement with the reported values (0.282306 ± 28, 2SD, n = 93) from solution analysis (Woodhead et al., 2004).

4. Results

4.1. Whole-rock major and trace elements

The major and trace element compositions of whole rocks are reported in Supp. Table 1. The Tongchang samples have Mg# of 61–70, 64.53–67.16 wt% SiO_2, 4.00–4.73 wt% Na_2O and 4.86–5.77 wt% K_2O. In comparison, the Shilicun samples have lower Mg# (36–41), slightly higher SiO_2 contents (67.32–68.13 wt%) but similar Na_2O (4.58–4.68 wt%) and K_2O contents (5.47–6.00 wt%). In the TAS diagram (Supp. Fig. 1a), the Tongchang samples are classified as quartz monzonite and granite, with most of the samples belonging to the alkaline series; the Shilicun samples are all classified as granite and all belong to the alkaline series. In the A.R. vs. SiO_2 diagram (Supp. Fig. 1b), the samples from both plutons all belong to the alkaline series. In the SiO_2 vs. K_2O diagram (Supp. Fig. 1c), the samples from both plutons all pot in the field of the shoshonitic series. The A/CNK values ($Al_2O_3/(CaO + Na_2O + K_2O)$, molar) of the samples from the Tongchang and Shilicun plutons are 0.78–1.02 and 0.88–0.89, respectively, indicating that they are all metaluminous granites (Supp. Fig. 1d).

The whole rocks of the Tongchang and Shilicun plutons have similar chondrite-normalized REE patterns, showing light REE enrichments and lack of Eu anomaly, and slightly higher abundances of light-middle REE in the former than the latter (Supp. Fig. 1e). The primitive mantle-normalized trace element patterns of whole rock samples from both plutons are also generally similar, showing enrichments in some large-ion-lithophile elements (LILE) such as Rb, Ba, K, Sr and Pb, and depletions in some high-field-strength elements (HFSE) such as Nb, Ta and Ti, thereby resulting in positive Pb anomaly and negative Nb-Ta-Ti anomalies. In more details, these two plutons have slightly different Th, U, Ta, Nb, Zr and Hf concentrations plus different Nb/Ta and Zr/Hf ratios (Supp. Fig. 1f and Supp. Table 1).

4.2. Zircon U—Pb age, trace element and Hf—O isotope data

Zircon U—Pb age, trace element and Hf—O isotope data and calculated parameters such as Ce^{4+}/Ce^{3+} ratios, and crystallization

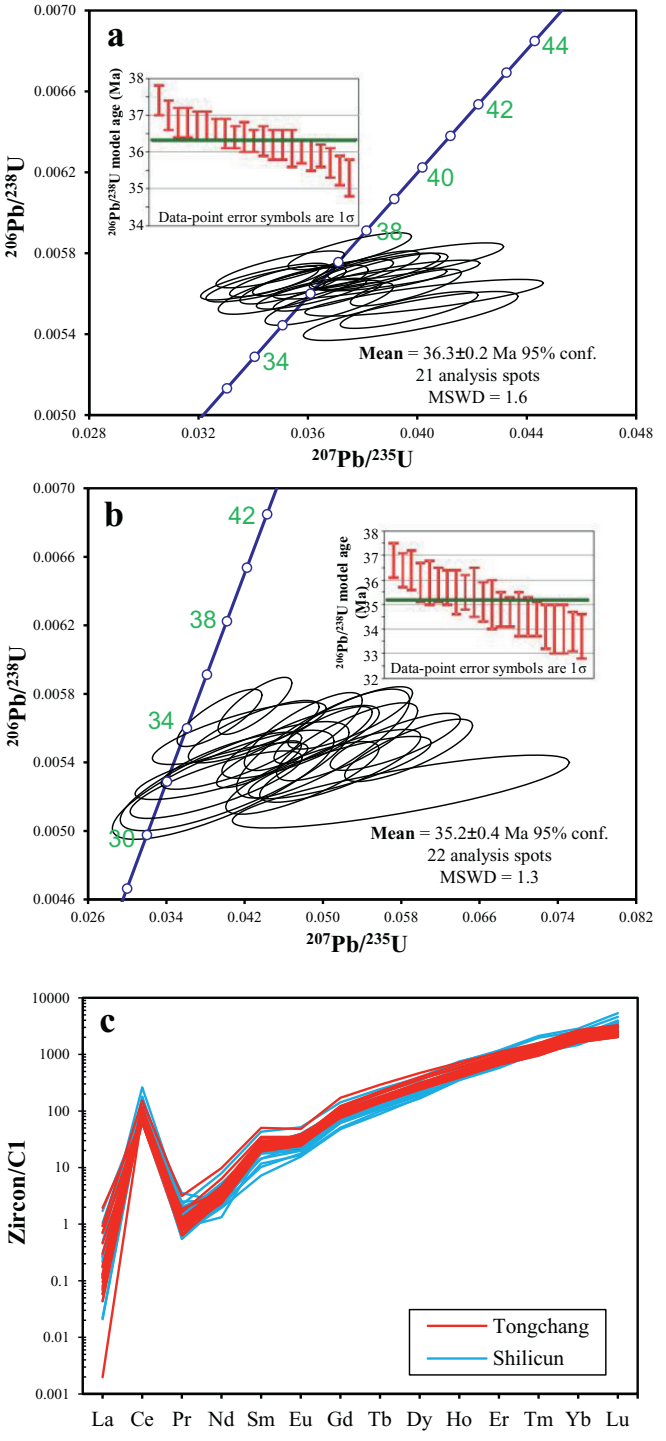

Fig. 5. LA-ICPMS zircon U—Pb concordia diagrams for the Tongchang (a) and Shilicun (b) plutons, and (c) Chondrite-normalized zircon REE patterns for the Tongchang and Shilicun plutons (normalization values from Sun and McDonough, 1989).

temperature based on Ti-in-zircon thermometry are presented in Supp. Table 2. The selected zircon grains from both plutons are mostly euhedral crystals with clear magmatic oscillatory zoning (Fig. 4a–b). Zircon crystals from the Tongchang pluton (sample TC917) contain 762–1729 ppm U and 354–1069 ppm Th, with Th/U from 0.38 to 0.78 that are within the range of typical magmatic zircon (Hartmann and Santos, 2004). The U—Pb isotopes of the selected zircon crystals from this pluton are concordant to nearly concordant, producing a weighted mean $^{206}Pb/^{238}U$ age of 36.3 ± 0.2 Ma (1σ, MSWD = 1.6, n = 21) (Fig. 5a). The zircon crystals from the Shilicun pluton (sample SLC11–2) contain 511–990 ppm U and 253–1001 ppm Th, with Th/U from 0.49 to 1.01 that are also within the range of typical magmatic zircon. The U—Pb isotopes of the selected zircon crystals from this pluton are concordant to nearly concordant, producing a weighted mean $^{206}Pb/^{238}U$ age of 35.2 ± 0.4 Ma (1σ, MSWD = 1.3, n = 22) (Fig. 5b). Our new zircon U—Pb ages for these two plutons are consistent with previous results. Xu et al. (2012) reported a zircon U—Pb age of 35.8 ± 0.2 Ma for the Tongchang pluton. Xia et al. (2005) reported a zircon U—Pb age of 36.8 ± 1.5 Ma for the Shilicun pluton.

The chondrite-normalized REE patterns of the dated magmatic zircon crystals from the Tongchang and Shilicun plutons are illustrated in Fig. 5c. The results show no significant differences in zircon REE compositions between these plutons. The zircon crystals from both plutons are all characterized by enrichments in heavy REE and depletions in light REE, plus positive Ce anomaly and weakly negative Eu anomaly.

The $^{176}Lu/^{177}Hf$, $^{176}Hf/^{177}Hf$ and $^{176}Yb/^{177}Yb$ ratios of the selected zircon crystals from the Tongchang pluton are from 0.000758 to 0.001729, from 0.282679 to 0.282730, and from 0.019317 to 0.046778, respectively. The $\varepsilon_{(Hf)}$ (t = 36.3 Ma) of 21 analyses are from −2.5 to −0.7, with a mean of −1.4 ± 1.0 (Fig. 6a) and the T_{DM2} model ages from 1157 to 1273 Ma. The $\delta^{18}O$ values of these zircon crystals vary from 6.3 to 7.1‰, with a mean value of 6.8 ± 0.4‰ (Fig. 6c). The selected zircon crystals (n = 18) from the Shilicun pluton have $^{176}Lu/^{177}Hf$ from 0.000841 to 0.001455, $^{176}Hf/^{177}Hf$ 0.282705 to 0.282788, and $^{176}Yb/^{177}Yb$ from 0.019429 to 0.036240. The calculated ε_{Hf} (t = 35.1 Ma) values are from −1.6 to 1.3, with a mean ε_{Hf} of −0.3 ± 1.8 (Fig. 6b) and the T_{DM2} model ages from1028 to 1215 Ma. Their $\delta^{18}O$ values are from 6.3 to 6.8‰, with a mean value of 6.5 ± 0.4‰ (Fig. 6d).

4.3. Quartz trace element data

No clear zoning is shown by CL images for the selected quartz crystals from the Tongchang and Shilicun plutons. Their trace element abundances and calculated crystallization pressures (P_{Ti}) based on the titanium-in-quartz thermobarometer are presented in Supp. Table 3. The selected quartz crystals from the Shilicun pluton have higher Li, Na, Al, Ti, Rb and Sr contents, and lower K, Sc and Sn contents, but similar Mg, Cr and Ge contents as compared to those from the Tongchang pluton. The calculated crystallization pressures (P_{Ti}) of quartz from the Shilicun pluton are from 7.52 to 14.3 kbar, with an average of 11.4 kbar. In contrast, the calculated crystallization pressures (P_{Ti}) of quartz from the Tongchang pluton are 2.08 to 3.61 kbar, with an average of 2.93 kbar, which are three times less than the values for the Shilicun pluton (Supp. Table 3 and Fig. 7a).

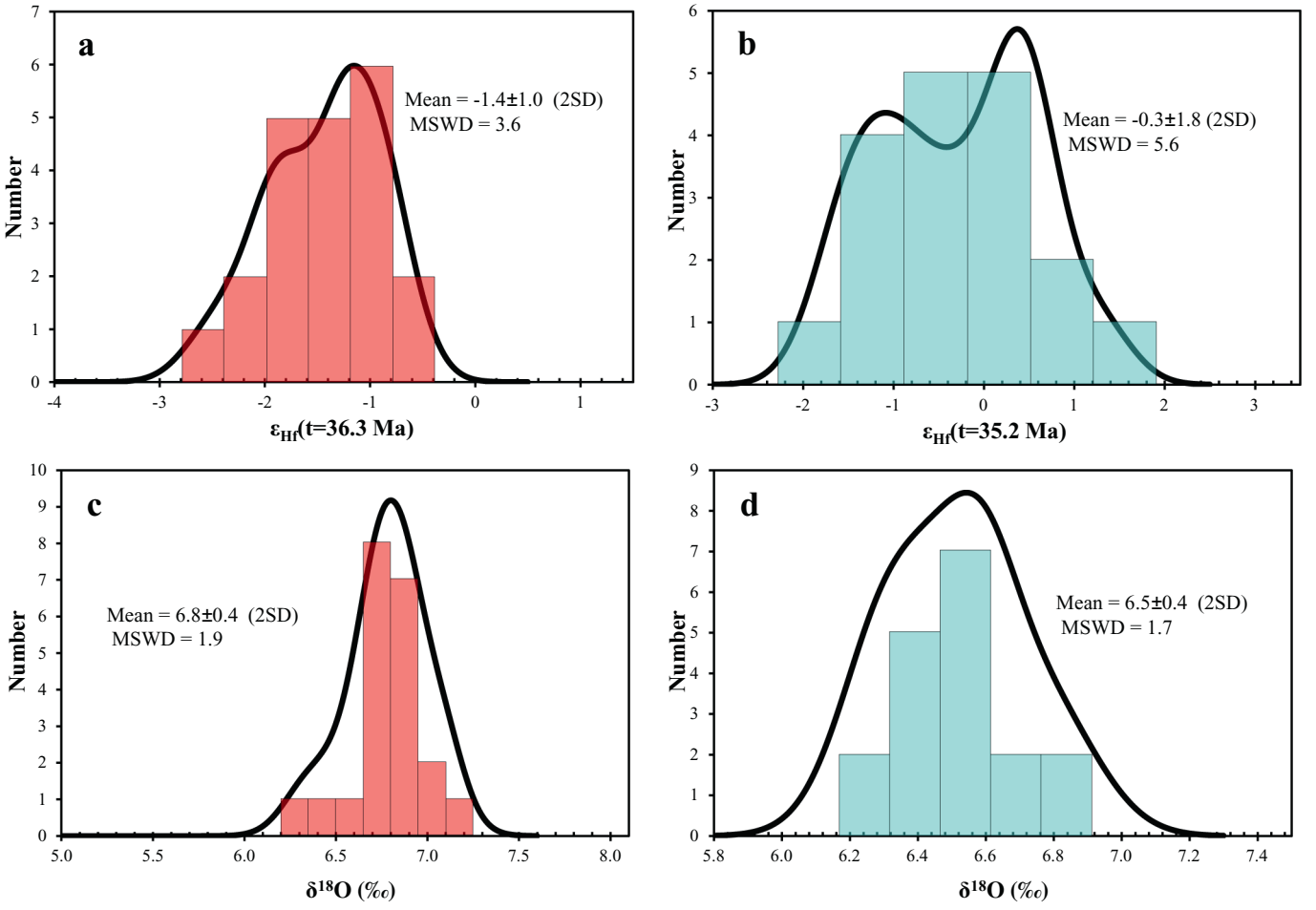

Fig. 6. Zircon initial Hf isotopic ($\varepsilon_{Hf}(t)$) histograms for the Tongchang (a) and Shilicun (b) plutons, and zircon oxygen isotopic ($\delta^{18}O$) histograms for the Tongchang (c) and Shilicun (d) plutons.

4.4. Plagioclase chemistry

The chemical compositions of plagioclase from the Tongchang and Shilicun plutons, determined by EMPA, are listed in Supp. Table 4. Plagioclase crystals from the Tongchang are exclusively oligoclase, with anorthite (An) contents from 15.8 to 28.7 mol%. Plagioclase crystals from the Shilicun plutons vary in composition from oligoclase to albite, with An contents from 6.0 to 13.9 mol% (Supp. Table 4). In addition to higher An contents, plagioclase crystals from the Tongchang pluton also have higher FeO than those from the Shilicun pluton (Fig. 7b and Supp. Table 4).

4.5. Apatite chemical and Sr—Nd isotopic compositions

The chemical compositions of apatite from the Tongchang and Shilicun plutons are listed in Supp. Table 5. The apatite Rb—Sr and Sm—Nd isotopic compositions are listed in Supp. Table 6. Apatite grains from the Tongchang pluton don't display clear magmatic oscillatory zoning, but those from the Shilicun pluton show clear magmatic oscillatory zoning (Fig. 4c–d). The apatite crystals from the Shilicun pluton contain <0.02 wt% Cl and from 0.26 to 0.45 wt% SO_3 (ave. 0.36 wt%). In contrast, The apatite crystals from the Tongchang pluton contain higher Cl (0.15–0.45 wt%, ave. 0.33 wt%) and lower SO_3 (0.11–0.29 wt%, ave. 0.23 wt%). As a result, the apatite crystals from the Tongchang pluton have higher chlorapatite (ClAp) and hydroxyapatite (HAp) components, plus higher Cl/F and OH/F ratios than those from the Shilicun pluton (Fig. 7c–d).

The apatite crystals from the Tongchang pluton have $^{87}Rb/^{86}Sr$ and $^{87}Sr/^{86}Sr$ ratios ranging from 0.0006 to 0.0024 and from 0.70690 to 0.70796, respectively, with corresponding initial $^{87}Sr/^{86}Sr$ (I_{Sr}, t = 36.3 Ma) range from 0.70690 to 0.70796, in good agreement with the whole-rock I_{Sr} (Xu et al., 2016a). These apatite crystals have $^{147}Sm/^{144}Nd$ and $^{143}Nd/^{144}Nd$ ratios range from 0.0992 to 0.1086 and from 0.512243 to 0.512249, respectively, with corresponding ε_{Nd} (t = 36.3 Ma) varying from −7.3 to −6.2, in good agreement with the whole-rock $\varepsilon_{Nd}(t)$ values (Xu et al., 2016a). The apatite crystals from the Shilicun pluton have $^{87}Rb/^{86}Sr$ ratios from 0.0004 to 0.0011 and $^{87}Sr/^{86}Sr$ ratios from 0.70703 to 0.70726, with corresponding I_{Sr} (t = 35.2 Ma) from 0.70703 to 0.70726, similar to the whole-rock I_{Sr} (Zhang and Xie, 1997). These apatite crystals have $^{147}Sm/^{144}Nd$ ratios from 0.0770 to 0.0899 and $^{143}Nd/^{144}Nd$ ratios from 0.512316 to 0.512404, with corresponding ε_{Nd} (t = 35.2 Ma) ranging from −5.8 to −4.0, similar to the whole-rock $\varepsilon_{Nd}(t)$ values (Zhang and Xie, 1997).

5. Discussion

5.1. Petrogenesis

Our zircon U—Pb age data show that the Tongchang and Shilicun plutons were emplaced in a short period between 36.3 ± 0.2 Ma and

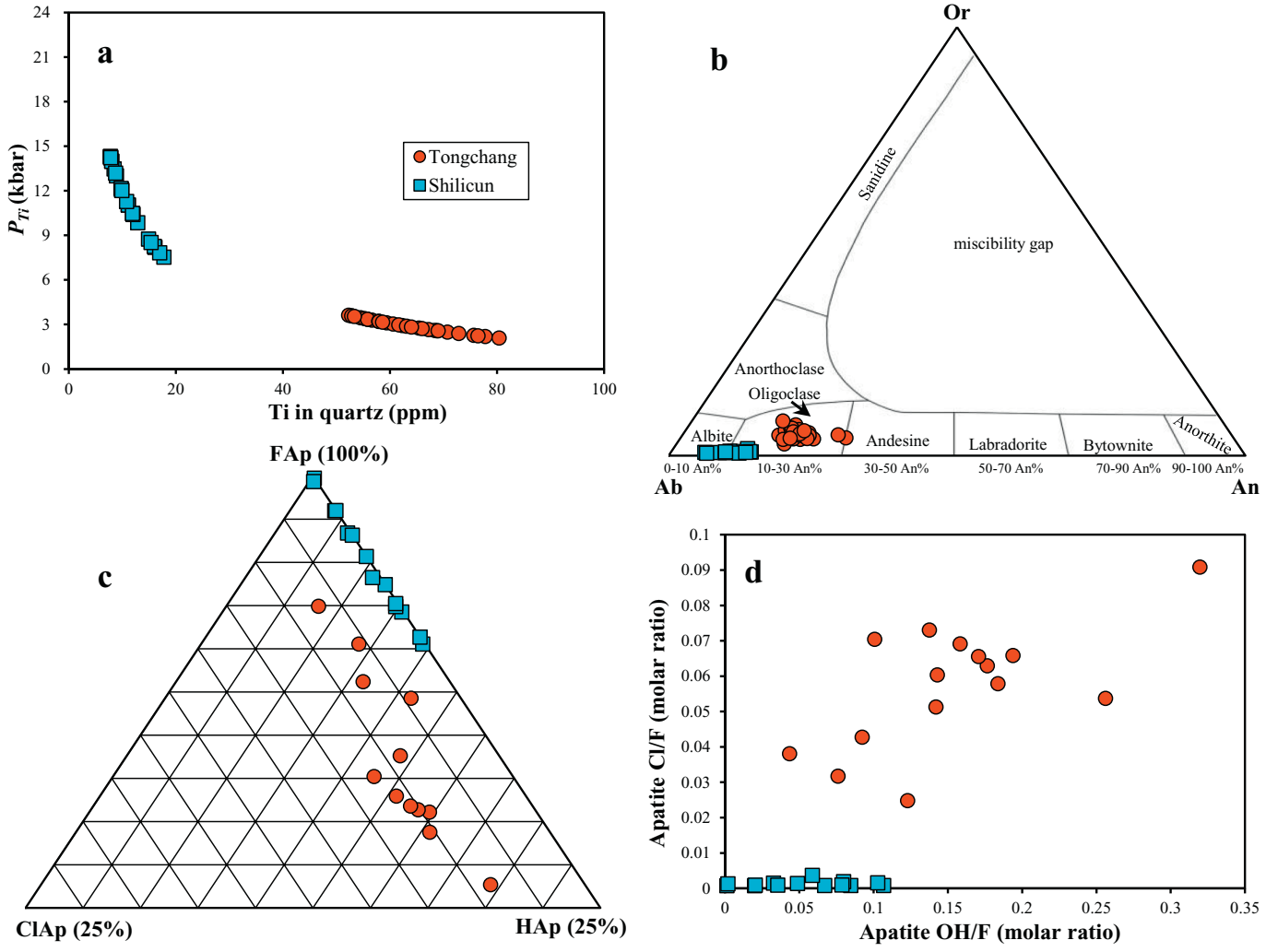

Fig. 7. Ti in quartz vs. P_{Ti} (a), plagioclase Or-Ab-An ternary (b), apatite FAp-ClAp-HAp ternary (a), and apatite OH/F vs. Cl/F (b) diagrams for the Tongchang and Shilicun plutons. Abbreviations: Or = orthoclase, Ab = albite, An = anorthite, FAp = fluorapatite, ClAp = chlorapatite, HAp = hydroxyapatite.

35.2 ± 0.4 Ma, broadly contemporaneous with the widespread potassic-ultrapotassic mafic-felsic magmatism in the Sanjiang region and in the western margin of the South China block (Hou et al., 2006; Lu et al., 2012, 2013a, 2013b; Xu et al., 2012). The distribution of these rocks is apparently controlled by some major strike-slip fault systems that are thought to be related to the protracted Indo-Asian continental collision that took place ~300 km to the west since ~65 Ma ago (Deng et al., 2014b). The collision event may have triggered lithospheric delamination and associated asthenosphere upwelling, producing the Cenozoic potassic-ultrapotassic mafic-felsic igneous rocks in the western Yangtze block (Hou et al., 2006, 2017; Lu et al., 2012, 2013a, 2013b; Xu et al., 2012, 2016a). In some areas, coeval alkaline granite plutons are also present or exclusive, such as the Tongchang and Shilicun plutons in the Ailaoshan area studied by us. The SiO_2 contents of these plutons are too high (65–68 wt%) for them to represent the compositions of any primary mantle-derived melt based on experimental results (e.g., Baker et al., 1995). As pointed out by these researchers, partial melting of a lithospheric mantle source cannot produce melts containing >57.3 wt% SiO_2. Some researchers choose a metasomatized lithosphere mantle source instead of a normal mantle source to explain the extremely high alkaline contents of the Cenozoic igneous rocks in the Sanjiang region (Hou et al., 2003; Jiang et al., 2006). Generally, this model may work for the mafic end-members of the alkaline suits but not for the felsic end-members, unless other processes such as high degrees of crustal contamination or extensive fractional crystallization, or the combination of these processes were involved (Miller et al., 1999). However, in the case of the Tongchang and Shilicun plutons, the mafic end-members, either present as separate intrusions in the area or as micro-enclaves within these plutons, have not been found. Therefore, it is unlikely that these plutons formed from the evolved liquids of magmas derived from a mantle source. Alternatively, they may have formed from crustal melts produced by mafic magma underplating. This model is also consistent with the chemical and isotopic compositions of the Tongchang and Shilicun plutons. As described above, the whole rocks of both plutons are characterized by significant light REE enrichments and pronounced negative Nb—Ta anomalies (Supp. Fig. 1e–f), which are similar to the average composition of the bulk crust (Rudnick and Gao, 2003). The Sr—Nd isotopes of these plutons are different from the ancient lower crust in the central part of the Yangtze Craton, i.e., the north-central part of the South China block (Fig. 8a; Jahn et al., 1999), but are similar to those of Neoproterozoic (zircon U—Pb age) amphibolite xenoliths entrained in some of the Cenozoic potassic felsic plutons in the northern part of the Ailaoshan shear zone such as the Liuhe pluton (Fig. 10a, Lu et al., 2013a, 2013b; Hou et al., 2017). As shown in Fig. 8b, Hf isotopes of the magmatic zircon crystals from the Tongchang and Shilicun plutons superimpose on the isotopic growth curves of the Neoproterozoic zircon crystals from the Liuhe amphibolite xenoliths as well as those from the Neoproterozoic mafic igneous rocks in the western margin of the Yangtze craton which stretches from Ailaoshan to Lijiang and farther north (Cai et al., 2014). The Neoproterozoic igneous rocks have arc trace element and isotope characteristics and are thought to be the products of Neoproterozoic subduction in this region (Cai et al., 2014; Zhao et al., 2008). The trace element and isotope compositions of the Cenozoic Tongchang and Shilicun granitic plutons from this study are consistent with melts produced by partial melting of the Neoproterozoic igneous rocks. Therefore, we propose that the parental magmas for these two plutons were derived from the underlying Neoproterozoic arc lower crust instead of a metasomatized lithospheric mantle thought previously (Xia et al., 2005; Xu et al., 2016a; Zhang and Xie, 1997).

5.2. Source variation between Tongchang and Shilicun

Higher zircon $\delta^{18}O$ values coupled with lower zircon $\varepsilon_{Hf}(t)$ and lower apatite $\varepsilon_{Nd}(t)$ values for the Tongchang pluton than those for the Shilicun pluton indicate more supracrustal contribution to the parental magma for the Tongchang pluton than that for the Shilicun pluton (Figs. 6 and 8; Plank and Langmuir, 1998; Valley et al., 1998; Dobosi et al., 2003; Roberts et al., 2013). This is consistent with higher whole-rock Th/Yb and Th/Nb ratios for the Tongchang pluton than those for the Shilicun pluton (Fig. 9a, Hawkesworth et al., 1997). This could have resulted from crustal assimilation or inherited from the source.

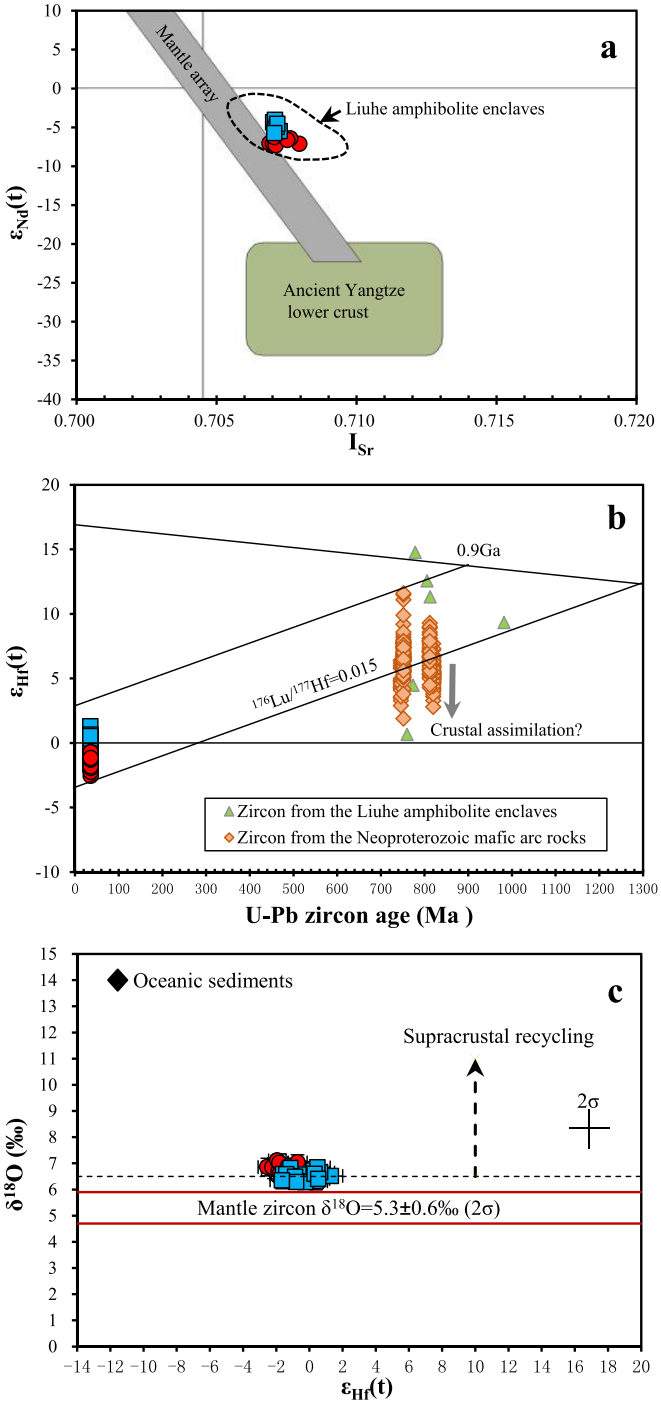

Fig. 8. Apatite I_{sr} vs. $\varepsilon_{Nd}(t)$ (a), zircon U—Pb age vs. $\varepsilon_{Hf}(t)$ (b), and zircon $\varepsilon_{Hf}(t)$ vs. $\delta^{18}O$ (c) diagrams for the Tongchang and Shilicun plutons. In Fig. 8a, data for the ancient Yangtze lower crust are from Jahn et al. (1999), and data for the Liuhe amphibolite enclaves are from Lu et al. (2013a). In Fig. 8b, data for zircon from the Liuhe amphibolite enclaves are from Hou et al. (2017) and data for zircon from the Neoproterozoic mafic arc rocks are from Zhao et al. (2008). In Fig. 8c, zircon $\delta^{18}O$ > 6.5‰ indicates significant incorporation of supracrustal material, and data for oceanic sediments are from Dobosi et al. (2003) and Roberts et al. (2013), and data for mantle zircon are from Valley et al. (1998).

As described above, the Tongchang intrusive rocks have lower SiO_2 contents, and higher whole-rock Mg# and An contents of plagioclase than the Shilicun intrusive rocks. This indicates that the parental magma for the Tongchang pluton is overall less evolved than that for the Shilicun pluton, which is the opposite of what to expect if these two plutons truly experienced different degrees of crustal assimilation. Thus, source variation seems more likely. We propose that the source rocks of the Tongchang pluton originated from a subarc mantle that contains more subducted sediments than the subarc mantle that produced the parental magma for the source rocks of the Shilicun pluton. Oceanic sediments commonly have high $\delta^{18}O$ coupled with low ε_{Hf} and low ε_{Nd} (Dobosi et al., 2003; Plank and Langmuir, 1998; Roberts et al., 2013).

The Tongchang and Shilicun plutons have Nb/Ta ratios lower and higher than that of the primitive mantle, respectively (Fig. 9b). Lack of correlation between whole-rock Nb/Ta ratios and TiO_2 contents for any of these plutons (Fig. 9b) indicate that the difference in Nb/Ta ratios between these plutons is not related to fractionation crystallization of Ti-bearing minerals such as rutile and amphibole (Xu et al., 2016a) but is more likely due to source variation in mineral phases. Based on the observed Nb/Ta ratios and experimental solid/melt partition coefficients for these elements under lower crustal conditions, the parental magma for the Tongchang pluton is consistent with melt derived from a shallow, hydrous mafic source (amphibolite or hornblende eclogite) whereas the parental magma for the Shilicun pluton is consistent with melt derived from a deeper, less hydrous mafic source (rutile eclogite) (Fig. 9b; Foley et al., 2002; Condie, 2005).

The whole-rock Nb/U ratios of the Tongchang and Shilicun plutons are lower than those of the continental lithospheric mantle, lower and upper continental crusts, and the average globally subducted sediment (Fig. 9c), suggesting that significant amounts of subducted slab-derived fluids (Nb/U ~0.22; Ayers, 1998) were likely added to the subarc mantle that produced the parental magma for the source rocks of these plutons. Lower whole-rock Nb/U ratios for the Tongchang pluton than the Shilicun pluton (Fig. 9c) may be due to larger amount of subducted slab-derived fluids being added to the subarc mantle that produced the parental magma for the source rocks of the Tongchang pluton than the Shilicun pluton. In brief, it appears that the Tongchang ore-bearing pluton originated from a shallower and more hydrous mafic source than the temporally and spatially associated Shilicun ore-barren pluton. Based on whole-rock Nb/U and Nb/Ta ratios, similar explanation was given previously to the occurrence of the Cenozoic Yulong ore-bearing granitic pluton and the coeval Nangqian ore-barren plutons in a small area in eastern Tibet (Fig. 9d, Xu et al., 2016a, 2016b).

5.3. Magma intrinsic variables and implications for ore genesis

The Ce^{4+}/Ce^{3+} of magmatic zircon is useful for estimating the oxidation state of parental magma for the zircon (Ballard et al., 2002). Calculated δK values of −1.9 to 0.7 (Supp. Table 2), largely <3, indicate that Ce^{4+}/Ce^{3+} ratios in zircon have good data quality and can be as a semi-quantitative oxygen fugacity method to reflect magma redox

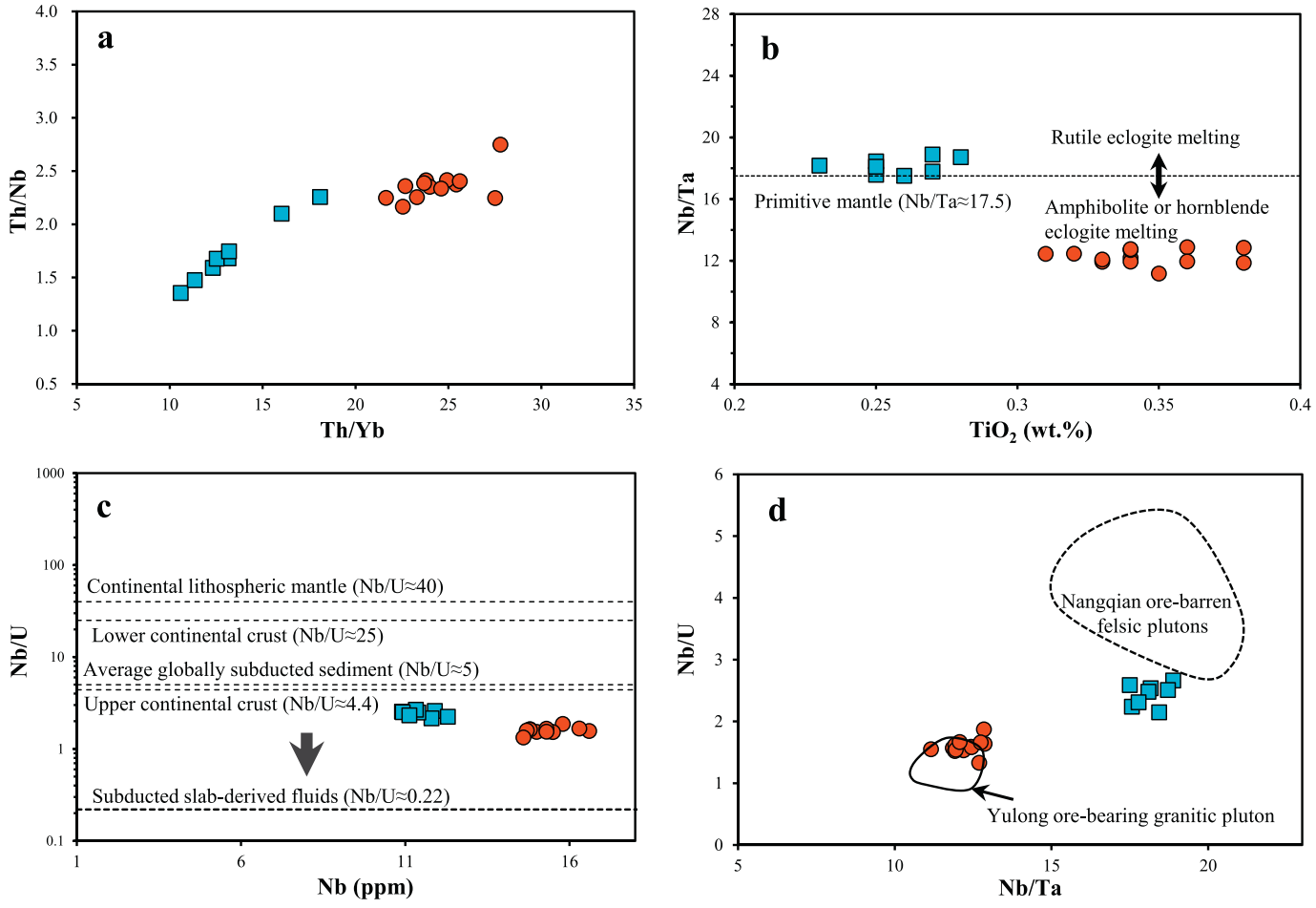

Fig. 9. Whole-rock Th/Yb vs. Th/Nb (a), TiO_2 vs. Nb/Ta (b), Nb vs. Nb/U (c), and Nb/Ta vs. Nb/U (d) diagrams for the Tongchang and Shilicun plutons. In Fig. 9b, Nb/Ta ratio for the Primitive mantle is from McDonough and Sun (1995), and trends for rutile eclogite melting and amphibolite or hornblende eclogite melting are from Foley et al. (2002). In Fig. 9c, Nb/U ratios for continental lithospheric mantle, upper and lower continental crusts, average globally subducted sediment, and subducted slab-derived fluids are from McDonough (1990), Rudnick and Gao (2003), Plank and Langmuir (1998) and Ayers (1998), respectively. Data scopes for the Yulong ore-bearing granitic and Nangqian ore-barren felsic plutons in Fig. 9d are from Xu et al. (2016a, 2016b).

states in this study (Zou et al., 2019). Magmatic zircon crystals from the Tongchang and Shilicun plutons all have Ce^{4+}/Ce^{3+} as high as those from some porphyry Cu deposits in northern Chile that formed from oxidized magmas in arc settings (Fig. 10a; Ballard et al., 2002). Our results also show that between the Tongchang and Shilicun plutons, the latter tends to have higher zircon Ce^{4+}/Ce^{3+} and whole-rock V/Sc ratios (Fig. 10a–b and Supp. Tables 1 and 2), indicating that the latter is more oxidized than the former (Ballard et al., 2002; Richards and Celâl Şengör, 2017). Likewise, higher apatite SO_3 contents, and lower apatite MnO contents for the Shilicun pluton than those for the Tongchang pluton (Fig. 10c and Supp. Table 5) reveal higher magma relative oxidation states for the former as well (Miles et al., 2014; Streck and Dilles, 1998), although these contents in apatite as redox proxies are debated (Konecke et al., 2017; Marks et al., 2016; Stokes et al., 2019). Collectively, these values indicate that the Shilicun ore-barren magmatic system was even more oxidized than the Tongchang ore-bearing magmatic system.

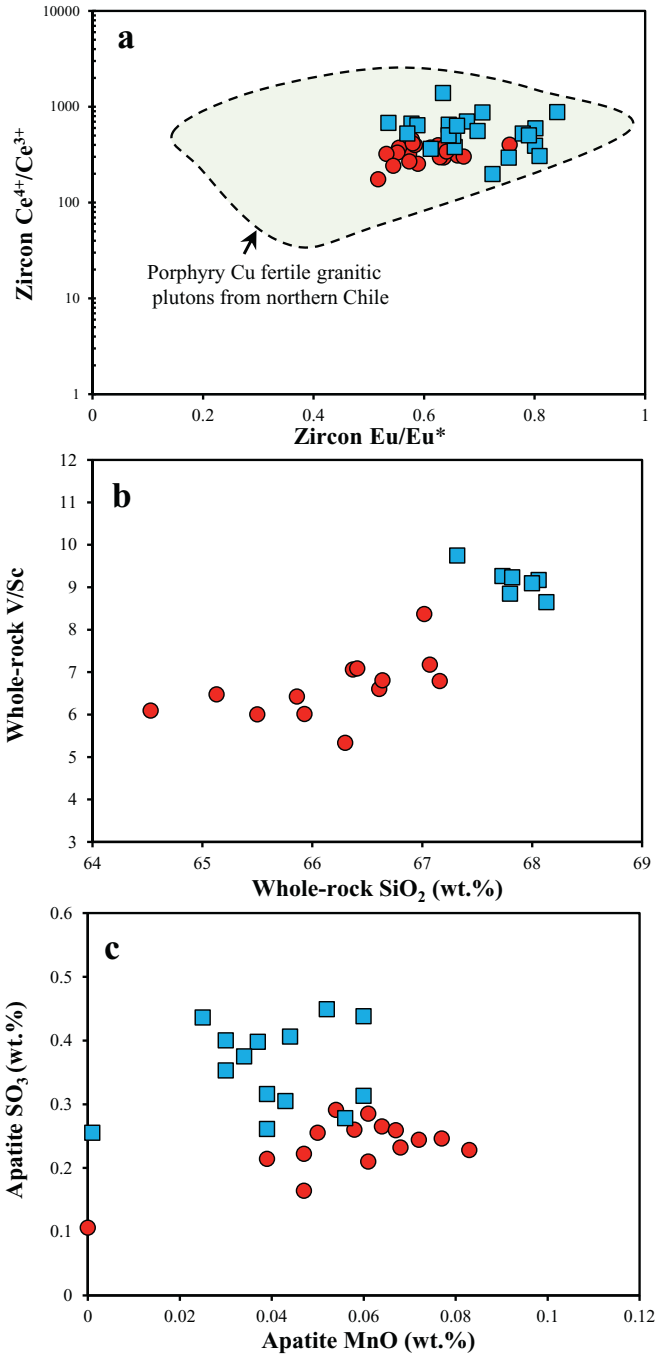

Fig. 10. Zircon Eu/Eu* vs. Ce^{4+}/Ce^{3+} (a), whole-rock SiO_2 vs. V/Sc (b), and apatite MnO vs. SO_3 (c) diagrams for the Tongchang and Shilicun plutons. Data scope for porphyry Cu fertile granitic plutons from northern Chile in Fig. 10a is from Ballard et al. (2002).

Another important difference between these two pluton is that the Tongchang ore-bearing pluton contains higher abundant amphibole and biotite than the Shilicun ore-barren pluton. This suggests that former likely formed from a more H_2O-rich melt than the Shilicun ore-barren pluton. Obviously, this is true only if whole rock H_2O contents are directly related to magma H_2O contents. Previous researchers suggested that this is often true for granitoids (Richards, 2011a; Wang et al., 2014c).

As shown in Fig. 7c, d, apatite crystals from the Tongchang ore-bearing pluton have higher hydroxylapatite (HAp) and chlorapatite (ClAp) contents, and higher molar OH/F and Cl/F ratios than those from the Shilicun ore-barren pluton. This may mainly reflect the higher OH/F and Cl/F ratios or H_2O-Cl contents in the parental melts for the Tongchang pluton, because the ratios of partition coefficients ($D_{OH}^{Ap\text{-}melt}/D_F^{Ap\text{-}melt}$, $D_{Cl}^{Ap\text{-}melt}/D_F^{Ap\text{-}melt}$) display much less variability, i.e., OH/F and Cl/F ratios in apatite are positively correlated with the corresponding ratios in the parental melts (McCubbin et al., 2015). Volatiles (Cl and H_2O) in magma will become progressively enriched as magma differentiation proceeds before saturation of the magma with an aqueous fluid phase (Audétat et al., 2000; Fu et al., 2008). This cannot explain the inferred higher magma Cl and H_2O contents for the Tongchang ore-bearing pluton than the Shilicun ore-barren pluton, because the parental magma for the latter is more evolved than that for the former based on plagioclase An and FeO compositions, whole-rock Mg# and Ti-in-zircon temperatures (Supp. Tables 1, 2 and 3) (Fu et al., 2008; Zhu et al., 2018). Variable degassing may be partially responsible for the observed differences (Ballard et al., 2002; Xu et al., 2016a), but no volcanic apparatuses served as magma degassing conduits are found to be associated either of the plutons.

Using the average crustal lithostatic pressure of 2.7 km per 1 kbar and the calculated lowest crystallization pressure of quartz described above, we have determined that the Shilicun and Tongchang plutons were emplaced at ~20.3 km and ~5.6 km, respectively. The value for the Tongchang pluton is significantly larger than that for typical porphyry systems (≤4 km; Richards, 2009). There are several possible causes for the discrepancy, the most important ones being (1) the quartz method used by us overestimates the crystallization pressure or (2) some of the selected quartz crystals are not in-situ crystallization products but rather entrained phenocrysts from greater depths. For these reasons, we cannot use the absolute values but only the relative values. We believe that it is reasonable to conclude that the emplacement depth of the Tongchang ore-bearing pluton is significantly shallower than that of the Shilicun ore-barren pluton.

Oxidized magmas are known to be important for the formation of porphyry Cu ± Mo ± Au ore deposits in the world (e.g., Ballard et al., 2002; Bi et al., 2009; Liang et al., 2006; Lu et al., 2016; Mungall, 2002; Shen et al., 2015; Sun et al., 2015, 2017; Wang et al., 2014a, 2014b; Xu et al., 2016a; Zhang et al., 2017). The results from this study are generally in good agreement with this but also reveal that oxidized magma alone does not guarantee the formation of a porphyry ore deposit. High H_2O and Cl contents in the magma and relatively shallow emplacement depth are also important. These are all understandable: oxidized magma has a better chance to be enriched chalcophile elements such as Cu, Mo and Au; H_2O-rich magma can provide more magmatic hydrothermal fluids; high Cl in magma results in high Cl contents in the magmatic hydrothermal fluid; Cl-bearing hydrothermal fluids have high capacity of transporting ore metals such as Cu, Mo and Au; shallower depth of magma emplacement reduce H_2O solubility in magma, facilitating fluid exsolution from the magma (Burnham, 1997; Richards, 2003, 2009, 2011a, 2011b, 2015; Sillitoe, 2010).

6. Conclusions

The results from this study support the notion that the Cenozoic Tongchang ore-bearing granitic pluton and the coeval Shilicun ore-barren granitic plutons in the Ailaoshan area could all be derived from the Neoproterozoic mafic arc lower crust, with the parental magma for the Tongchang pluton from a shallower and more hydrous source than that for the Shilicun pluton. Our new data also indicate some other important differences between the ore-bearing and ore-barren plutons. Both of them appear to have formed from felsic magmas that are as oxidized as those for some porphyry Cu ± Mo ± Au ore deposits in northern Chile, but the parental magma for the Shilicun ore-barren pluton is slightly more oxidized than that for the Tongchang ore-bearing pluton based on our estimation. Such a surprising result suggests that highly oxidized felsic magma alone does not guarantee the formation of a porphyry Cu ± Mo ± Au ore deposit. High H_2O and Cl contents in the magma plus relatively shallow depth of emplacement depth are also important for the formation of this type of deposit.

Acknowledgements

This research was jointly funded by the Natural Science Foundation of China (41473052, 41873052), the Strategic Priority Research Program (B) of the Chinese Academy of Sciences (XDB18000000), the National Basic Research Program (2015CB452603), the Team of the Belt and Road of the Chinese Academy of Sciences and the 100 Innovative Talents of Guizhou province to Xian-Wu Bi. We thank Profs Xian-Hua Li and Yue-Heng Yang for their advice in zircon oxygen isotopic and apatite Rb—Sr isotopic analysis, respectively, Prof. Zhao-Chu Hu for his assistance in zircon Hf isotopic analysis, and Drs. Yi Hu and Carl Spandler for their help in apatite Sm—Nd isotopic analysis. We are indebted to Dr. Chusi Li of Indiana University who provided much-needed scientific and English edits to the manuscript. Constructive comments from Dr. Rui Wang and an anonymous reviewer as well as insightful guidance from Editor-in-Chief Prof. Xian-Hua Li are greatly appreciated.

Appendix A. Supplementary data

Supplementary data to this article can be found online at https://doi.org/10.1016/j.lithos.2019.03.031.

References

Audétat, A., Günther, D., Heinrich, C.A., 2000. Magmatic-hydrothermal evolution in a fractionating granite: a microchemical study of the Sn-W-F-mineralized Mole Granite (Australia). Geochim. Cosmochim. Acta 64, 3373–3393.

Audétat, A., Garbe-Schoenberg, D., Kronz, A., Pettke, T., Rusk, B., Donovan, J.J., Lowers, H.A., 2015. Characterisation of a natural quartz crystal as a reference material for microanalytical determination of Ti, Al, Li, Fe, Mn, Ga and Ge. Geostand. Geoanal. Res. 39, 171–184.

Ayers, J., 1998. Trace element modeling of aqueous fluid–peridotite interaction in the mantle wedge of subduction zones. Contrib. Mineral. Petrol. 132, 390–404.

Baker, M., Hirschmann, M., Ghiorso, M., Stolper, E., 1995. Compositions of near-solidus peridotite melts from experiments and thermodynamic calculations. Nature 375, 308–311.

Ballard, J.R., Palin, J.M., Campbell, I.H., 2002. Relative oxidation states of magmas inferred from Ce(IV)/Ce(III) in zircon: application to porphyry copper deposits of northern Chile. Contrib. Mineral. Petrol. 144, 347–364.

Bi, X.W., Hu, R.Z., Hanley, J.J., Mungall, J., Peng, J.T., Shang, L.B., Wu, K.X., Suang, Y., Li, H.L., Hu, X.Y., 2009. Crystallisation conditions (T, P, fO_2) from mineral chemistry of Cu- and Au-mineralised alkaline intrusions in the Red River-Jinshajiang alkaline igneous belt, western Yunnan Province, China. Mineral. Petrol. 96, 43–58.

Burnham, C.W., 1997. Magmas and hydrothermal fluids. In: Barnes, H.L. (Ed.), Geochemistry of Hydrothermal Ore Deposits, 3rd ed. John Wiley and Sons, New York, pp. 63–123.

Cai, Y., Wang, Y., Cawood, P.A., Fan, W., Liu, H., Xing, X., Zhang, Y., 2014. Neoproterozoic subduction along the Ailaoshan zone, South China: geochronological and geochemical evidence from amphibolite. Precambrian Res. 245, 13–28.

Condie, K.C., 2005. TTGs and adakites: are they both slab melts? Lithos 80, 33–44.

Deng, J., Wang, Q., Li, G., Li, C., Wang, C., 2014a. Tethys tectonic evolution and its bearing on the distribution of important mineral deposits in the Sanjiang region, SW China. Gondwana Res. 26, 419–437.

Deng, J., Wang, Q., Li, G., Santosh, M., 2014b. Cenozoic tectono-magmatic and metallogenic processes in the Sanjiang region, southwestern China. Earth Sci. Rev. 138, 268–299.

Dobosi, G., Kempton, P.D., Downes, H., Embey-Isztin, A., Thirlwall, M., Greenwood, P., 2003. Lower crustal granulite xenoliths from the Pannonian Basin, Hungary, part 2: Sr-Nd-Pb-Hf and O isotope evidence for formation of continental lower crust by tectonic emplacement of oceanic crust. Contrib. Mineral. Petrol. 144, 671–683.

Fisher, C.M., McFarlane, C.R.M., Hanchar, J.M., Schmitz, M.D., Sylvester, P.J., Lam, R., Longerich, H.P., 2011. Sm-Nd isotope systematics by laser ablation-multicollector-inductively coupled masss pectrometry: methods and potential natural and synthetic reference materials. Chem. Geol. 284, 1–20.

Foley, S., Tiepolo, M., Vannucci, R., 2002. Growth of early continental crust controlled by melting of amphibolite in subduction zones. Nature 417, 837–840.

Fu, B., Page, F.Z., Cavosie, A.J., Fournelle, J., Kita, N.T., Lackey, J.S., Wilde, S.A., Valley, J.W., 2008. Ti-in-zircon thermometry: applications and limitations. Contrib. Mineral. Petrol. 156, 197–215.

Hammerli, J., Kemp, A.I.S., Spandler, C., 2014. Neodymium isotope equilibration during crustal metamorphism revealed by in situ microanalysis of REE-rich accessory minerals. Earth Planet. Sci. Lett. 392, 133–142.

Hartmann, L.A., Santos, J.O.S., 2004. Predominance of high Th/U, magmatic zircon in Brazilian Shield sandstones. Geology 32, 73–76.

Hawkesworth, C., Turner, S., Peate, D., McDermott, F., VanCalsteren, P., 1997. Elemental U and Th variations in island arc rocks: implications for U-series isotopes. Chem. Geol. 139, 207–221.

Hou, Z.Q., Ma, H.W., Zaw, K., Zhang, Y.Q., Wang, M.J., Wang, Z., Pan, G.T., Tang, R.L., 2003. The Himalayan Yulong porphyry copper belt: product of large-scale strikeslip faulting in eastern Tibet. Econ. Geol. 98, 125–145.

Hou, Z.Q., Zeng, P.S., Gao, Y.F., Du, A.D., Fu, D.M., 2006. Himalayan Cu-Mo-Au mineralization in the eastern Indo-Asian collision zone: constraints from Re-Os dating of molybdenite. Mineral. Deposita 41, 33–45.

Hou, Z.Q., Zaw, K., Pan, G.T., Mo, X.X., Xu, Q., Hu, Y.Z., Li, X.Z., 2007. Sanjiang Tethyan metallogenesis in SW China: tectonic setting, metallogenic epochs and deposit types. Ore Geol. Rev. 31, 48–87.

Hou, Z., Zhou, Y., Wang, R., Zheng, Y., He, W., Zhao, M., Evans, N.J., Weinberg, R.F., 2017. Recycling of metal-fertilized lower continental crust: origin of non-arc Au-rich porphyry deposits at cratonic edges. Geology 45, 563–566.

Hu, R.Z., Burnard, P.G., Bi, X.W., Zhou, M.F., Pen, J.T., Su, W.C., Wu, K.X., 2004. Helium and argon isotope geochemistry of alkaline intrusion-associated gold and copper deposits along the Red River-Jinshajiang fault belt, SW China. Chem. Geol. 203, 305–317.

Hu, Z.C., Liu, Y.S., Gao, S., Liu, W.G., Yang, L., Zhang, W., Tong, X.R., Lin, L., Zong, K.Q., Li, M., Chen, H.H., Zhou, L., 2012. Improved in situ Hf isotope ratio analysis of zircon using newly designed X skimmer cone and Jet sample cone in combination with the addition of nitrogen by laser ablation multiple collector ICP-MS. J. Anal. At. Spectrom. 27, 1391–1399.

Jahn, B.M., Wu, F.Y., Lo, C.H., Tsai, C.H., 1999. Crust-mantle interaction induced by deep subduction of the continental crust: Geochemical and Sr-Nd isotopic evidence from post-collisional mafic–ultramafic intrusions of the northern Dabie complex, central China. Chem. Geol. 157, 119–146.

Jiang, Y.H., Jiang, S.Y., Ling, H.F., Dai, B.Z., 2006. Low-degree melting of metasomatized lithospheric mantle for the origin of Cenozoic Yulong monzogranite-porphyry, east Tibet: geochemical and Sr–Nd–Pb–Hf isotopic constraints. Earth Planet. Sci. Lett. 241, 617–633.

Konecke, B.A., Fiege, A., Simon, A.C., Parat, F., Stechern, A., 2017. Co-variability of S^{6+}, S^{4+}, and S^{2-} in apatite as a function of oxidation state: implications for a new oxybarometer. Am. Mineral. 102, 548–557.

Lan, T.-G., Hu, R.-Z., Bi, X.-W., Mao, G.-J., Wen, B.-J., Liu, L., Chen, Y.-H., 2018. Metasomatized asthenospheric mantle contributing to the generation of Cu-Mo deposits within an intracontinental setting: a case study of the similar to 128 Ma Wangjiazhuang Cu-Mo deposit, eastern North China Craton. J. Asian Earth Sci. 160, 460–489.

Li, X., Li, W., Wang, X., Li, Q., Liu, Y., Tang, G., 2009. Role of mantle-derived magma in genesis of early Yanshanian granites in the Nanling Range, South China: In situ zircon Hf-O isotopic constraints. Sci. China Ser. D Earth Sci. 52, 1262–1278.

Liang, H.Y., Campbell, I.H., Allen, C., Sun, W.D., Liu, C.Q., Yu, H.X., Xie, Y.W., Zhang, Y.Q., 2006. Zircon Ce^{4+}/Ce^{3+} ratios and ages for Yulong ore-bearing porphyries in eastern Tibet. Mineral. Deposita 41, 152–159.

Liu, Y.S., Hu, Z.C., Zong, K.Q., Gao, C.G., Gao, S., Xu, J.A., Chen, H.H., 2010. Reappraisement and refinement of zircon U–Pb isotope and trace element analyses by LA–ICP–MS. Chin. Sci. Bull. 55, 1535–1546.

Lu, Y.J., Kerrich, R., Cawood, P.A., McCuaig, T.C., Hart, C.J.R., Li, Z.X., Hou, Z.Q., Bagas, L., 2012. Zircon SHRIMP U-Pb geochronology of potassic felsic intrusions in western Yunnan, SW China: Constraints on the relationship of magmatism to the Jinsha suture. Gondwana Res. 22, 737–747.

Lu, Y.J., Kerrich, R., Kemp, A.I.S., McCuaig, T.C., Hou, Z.Q., Hart, C.J.R., Li, Z.X., Cawood, P.A., Bagas, L., Yang, Z.M., Cliff, J., Belousova, E.A., Jourdan, F., Evans, N.J., 2013a. Intracontinental eocene-oligocene porphyry cu mineral systems of Yunnan, Western Yangtze Craton, China: compositional characteristics, sources, and implications for continental collision metallogeny. Econ. Geol. 108, 1541–1576.

Lu, Y.J., Kerrich, R., McCuaig, T.C., Li, Z.X., Hart, C.J.R., Cawood, P.A., Hou, Z.Q., Bagas, L., Cliff, J., Belousova, E.A., Tang, S.H., 2013b. Geochemical, Sr-Nd-Pb, and zircon Hf-O isotopic compositions of eocene-oligocene shoshonitic and potassic adakite-like felsic intrusions in Western Yunnan, SW China: petrogenesis and tectonic implications. J. Petrol. 54, 1309–1348.

Lu, Y.J., Loucks, R.R., Fiorentini, M., Campbell, M.T., Evans, N.J., Yang, Z.M., Hou, Z.Q., Kirkland, C.L., Parra-Avila, L.A., Kobussen, A., 2016. Zircon Compositions as a Pathfinder for Porphyry Cu ± Mo ± Au Deposits. vol. 19. Society of Economic Geologists, Inc, pp. 329–347 Special Publication.

Marks, M.A.W., Scharrer, M., Ladenburger, S., Markl, G., 2016. Comment on "Apatite: A new redox proxy for silicic magmas?" [Geochimica et Cosmochimica Acta 132 (2014) 101-119]. Geochim. Cosmochim. Acta 183, 267–270.
McDonough, W.F., Sun, S.-s., 1995. The composition of the Earth. Chem. Geol. 120, 223–253.
McCubbin, F.M., Kaaden, K.E.V., Tartèse, R., Boyce, J.W., Mikhail, S., Whitson, E.S., Bell, A.S., Anand, M., Franchi, I.A., Wang, J., 2015. Experimental investigation of F, Cl, and OH partitioning between apatite and Fe-rich basaltic melt at 1.0–1.2 GPa and 950–1000 C. Am. Mineral. 100, 1790–1802.
McDonough, W.F., 1990. Constraints on the compositions of the continental lithospheric mantle. Earth Planet. Sci. Lett. 101, 1–18.
Miles, A.J., Graham, C.M., Hawkesworth, C.J., Gillespie, M.R., Hinton, R.W., Bromiley, G.D., Emmac, 2014. Apatite: a new redox proxy for silicic magmas? Geochim. Cosmochim. Acta 132, 101–119.
Miller, C., Schuster, R., Klötzli, U., Frank, W., Purtscheller, F., 1999. Post-collisional potassic and ultrapotassic magmatism in SW Tibet: geochemical and Sr–Nd–Pb–O isotopic constraints for mantle source characteristics and petrogenesis. J. Petrol. 40, 1399–1424.
Mungall, J.E., 2002. Roasting the mantle: Slab melting and the genesis of major Au and Au-rich Cu deposits. Geology 30, 915 Apatite: A New Redox Proxy for Silicic Magmas?, p. 918.
Plank, T., Langmuir, C.H., 1998. The chemical composition of subducting sediment and its consequences for the crust and mantle. Chem. Geol. 145, 325–394.
Richards, J.P., 2003. Tectono-magmatic precursors for porphyry Cu-(Mo-Au) deposit formation. Econ. Geol. Bull. Soc. Econ. Geol. 98, 1515–1533.
Richards, J.P., 2009. Postsubduction porphyry Cu-Au and epithermal Au deposits: products of remelting of subduction-modified lithosphere. Geology 37, 247–250.
Richards, J.P., 2011a. High Sr/Y magmas and porphyry Cu±Mo±Au deposits: just add water. Econ. Geol. 106, 1075–1081.
Richards, J.P., 2011b. Magmatic to hydrothermal metal fluxes in convergent and collided margins. Ore Geol. Rev. 40, 1–26.
Richards, J.P., 2015. The oxidation state, and sulfur and Cu contents of arc magmas: implications for metallogeny. Lithos 233, 27–45.
Richards, J.P., Celâl Şengör, A.M., 2017. Did Paleo-Tethyan anoxia kill arc magma fertility for porphyry copper formation? Geology 45, 591–594.
Roberts, N.M.W., Slagstad, T., Parrish, R.R., Norry, M.J., Marker, M., Horstwood, M.S.A., 2013. Sedimentary recycling in arc magmas: Geochemical and U-Pb-Hf-O constraints on the Mesoproterozoic Suldal Arc, SW Norway. Contrib. Mineral. Petrol. 165, 507–523.
Rudnick, R.L., Gao, S., 2003. Composition of the continental crust. In: Holland, H.D., Turekian, K.K. (Eds.), Treatise on Geochemistry. Elsevier-Pergamon, Oxford, pp. 1–64.
Shen, P., Hattori, K., Pan, H., Jackson, S., Seitmuratova, E., 2015. Oxidation condition and metal fertility of granitic magmas: zircon trace-element data from porphyry Cu Deposits in the Central Asian orogenic belt. Econ. Geol. 110, 1861–1878.
Sillitoe, R.H., 2010. Porphyry copper systems. Econ. Geol. 105, 3–41.
Stokes, T.N., Bromiley, G.D., Potts, N.J., Saunders, K.E., Miles, A.J., 2019. The effect of melt composition and oxygen fugacity on manganese partitioning between apatite and silicate melt. Chem. Geol. 506, 162–174.
Streck, M.J., Dilles, J.H., 1998. Sulfur evolution of oxidized arc magmas as recorded in apatite from a porphyry copper batholith. Geology 26, 523–526.
Sun, S.S., McDonough, W.F., 1989. Chemical and isotopic systematics of oceanic basalts: Implications for mantle composition and processes. Geol. Soc. Lond. Spec. Publ. 42, 313–345.
Sun, W., Huang, R.f., Li, H., Hu, Y.b., Zhang, C.c., Sun, S.j., Zhang, L.p., Ding, X., Li, C.y., Zartman, R.E., Ling, M.x., 2015. Porphyry deposits and oxidized magmas. Ore Geol. Rev. 65, 97–131.
Sun, W., Wang, J.t., Zhang, L.p., Zhang, C.c., Li, H., Ling, M.X., Ding, X., Li, C.Y., Liang, H.Y., 2017. The formation of porphyry copper deposits. Acta Geochim. 36, 9–15.
Valley, J.W., Kinny, P.D., Schulze, D.J., Spicuzza, M.J., 1998. Zircon megacrysts from kimberlite: oxygen isotope variability among mantle melts. Contrib. Mineral. Petrol. 133, 1–11.
Wang, F., Liu, S.A., Li, S., Akhtar, S., He, Y., 2014a. Zircon U-Pb ages, Hf-O isotopes and trace elements of Mesozoic high Sr/Y porphyries from Ningzhen, eastern China: constraints on their petrogenesis, tectonic implications and Cu mineralization. Lithos 200, 299–316.
Wang, R., Richards, J.P., Hou, Z.q., Yang, Z.m., Gu, Z.b., DuFrane, S.A., 2014b. Increasing magmatic oxidation state from paleocene to miocene in the Eastern Gangdese Belt, Tibet: Implication for collision-related porphyry Cu-Mo +/− Au mineralization. Econ. Geol. 109, 1943–1965.
Wang, R., Richards, J.P., Hou, Z.Q., Yang, Z.M., DuFrane, S.A., 2014c. Increased magmatic water content-the key to Oligo-Miocene porphyry Cu-Mo±Au formation in the eastern Gangdese belt, Tibet. Econ. Geol. 195, 1315–1339.
Wang, R., Weinberg, R.F., Collins, W.J., Richards, J.P., Zhu, D.-c., 2018. Origin of postcollisional magmas and formation of porphyry Cu deposits in southern Tibet. Earth Sci. Rev. 181, 122–143.
Woodhead, J., Hergt, J., Shelley, M., Eggins, S., Kemp, R., 2004. Zircon Hf-isotope analysis with an excimer laser, depth profiling, ablation of complex geometries, and concomitant age estimation. Chem. Geol. 209, 121–135.
Xia, B., Lin, Q.C., Zhang, Y.Q., 2005. Zircon SHRIMP dating of diopside granite in Ailaoshan-Jinshajiang rock belt and its geological implications—Example for Yuzhaokuai, Matouwan and Shilicun diopside granites. Geotecton. Metallog. 29, 35–43 (in Chinese with English abstract).
Xie, Y.W., Zhang, Y.Q., 1988. The characteristics and origin of diopside granite in Shilicun, Yunan. Geochimica 4, 301–309 (in Chinese with English abstract).
Xu, L.L., Bi, X.W., Hu, R.Z., Zhang, X.C., Su, W.C., Qu, W.J., Hu, Z.C., Tang, Y.Y., 2012. Relationships between porphyry Cu–Mo mineralization in the Jinshajiang–Red River metallogenic belt and tectonic activity: constraints from zircon U–Pb and molybdenite Re–Os geochronology. Ore Geol. Rev. 48, 460–473.
Xu, L.L., Bi, X.W., Hu, R.Z., Tang, Y.Y., Jiang, G.H., Qi, Y.Q., 2014. Origin of the ore-forming fluids of the Tongchang porphyry Cu–Mo deposit in the Jinshajiang–Red River alkaline igneous belt, SW China: constraints from He, Ar and S isotopes. J. Asian Earth Sci. 79, 884–894.
Xu, L.L., Bi, X.W., Hu, R.Z., Qi, Y.Q., Tang, Y.Y., Wang, X.S., Zhu, J.J., 2016a. Redox states and genesis of magmas associated with intra-continental porphyry Cu-au mineralization within the Jinshajiang-Red River alkaline igneous belt, SW China. Ore Geol. Rev. 73, 330–345.
Xu, Y., Bi, X.W., Hu, R.Z., Chen, Y.W., Liu, H.Q., Xu, L.L., 2016b. Geochronology and geochemistry of Eocene potassic felsic intrusions in the Nangqian basin, eastern Tibet: tectonic and metallogenic implications. Lithos 246–247, 212–227.
Yang, Y.H., Wu, F.Y., Yang, J.H., Chew, D.M., Xie, L.W., Chu, Z.Y., Zhang, Y.B., Huang, C., 2014. Sr and Nd isotopic compositions of apatite reference materials used in U-Th-Pb geochronology. Chem. Geol. 385, 35–55.
Zhang, Y.Q., Xie, Y.W., 1997. Nd, Sr isotopic characteristics and chronology of Ailaoshan–Jinshajiang alkali-rich intrusions. Sci. China (Ser. D) 27, 289–293 (in Chinese).
Zhang, C.c., Sun, W.d., Wang, J.t., Zhang, L.p., Sun, S.j., Wu, K., 2017. Oxygen fugacity and porphyry mineralization: a zircon perspective of Dexing porphyry Cu deposit, China. Geochim. Cosmochim. Acta 206, 343–363.
Zhao, J.H., Zhou, M.F., Yan, D.P., Yang, Y.H., Sun, M., 2008. Zircon Lu–Hf isotopic constraints on Neoproterozoic subduction-related crustal growth along the western margin of the Yangtze Block, South China. Precambrian Res. 163, 189–209.
Zhu, J.J., Hu, R., Richards, J.P., Bi, X., Zhong, H., 2015. Genesis and Magmatic-Hydrothermal Evolution of the Yangla Skarn Cu Deposit, Southwest China. Econ. Geol. 110, 631–652.
Zhu, J.J., Richards, J.P., Rees, C., Creaser, R., DuFrane, S.A., Locock, A., Petrus, J.A., Lang, J., 2018. Elevated magmatic sulfur and chlorine contents in ore-forming magmas at the red chris porphyry Cu-Au deposit, Northern British Columbia, Canada. Econ. Geol. 113, 1047–1075.
Zou, X., Qin, K., Han, X., Li, G., Evans, N.J., Li, Z., Yang, W., 2019. Insight into zircon REE oxy-barometers: a lattice strain model perspective. Earth Planet. Sci. Lett. 506, 87–96.